IEEE Access
Multidisciplinary | Rapid Review | Open Access Journal

Received December 11, 2019, accepted December 24, 2019, date of publication December 30, 2019,
date of current version January 9, 2020.

Digital Object Identifier 10.1109/ACCESS.2019.2963079

Anti-Disturbance Control Based on Cascade ESO and Sliding Mode Control for Gimbal System of Double Gimbal CMG

HAITAO LI AND JIANGKUN YU
School of Instrumentation Science and Optoelectronics Engineering, Beihang University, Beijing 100191, China
Corresponding author: Haitao Li (haitaoli@buaa.edu.cn)

This work was supported by the National Natural Science Foundation of China under Grant 61773038.

ABSTRACT Disturbance torque and unmodeled dynamics are the main important factors which affect the angular velocity precision of a gimbal system in double gimbal control moment gyro (DGCMG). In this paper, a compound control method combining reduced-order cascade extended state observer (RCESO) and integral sliding mode control (SMC) is proposed, aiming at effectively eliminating the influence of exogenous disturbances and unmodeled dynamics, and achieving high precision angular velocity control of the gimbal system. Firstly, the disturbance torque is observed by the RCESO, and the parameter tuning method of RCESO is studied. Secondly, to enhance the robustness of the whole control system and take into account disturbance estimation errors, an integral sliding mode control is introduced. Simulation and experimental results show that the proposed control method not only improves the compensation performance of the gimbal system with external disturbances, but also enhances the robustness and improves the angular velocity precision of the gimbal system.

INDEX TERMS DGCMG, gimbal system, RCESO, parameter configuration, integral sliding mode.

I. INTRODUCTION

Control moment gyro (CMG) has the advantages of large output torque, good dynamic performance and high control accuracy, making it the preferred actuator of attitude control for large spacecraft [1], [2]. According to the degree of freedom of the gimbal, it can be divided into single gimbal CMG (SGCMG) and double gimbal CMG (DGCMG) [3]. One DGCMG can afford two freedom torque and has better singularity avoidance properties, making it very attractive for attitude control systems of space stations and satellites [4]. DGCMG is mainly composed of high-speed rotor system and inner and outer gimbal system. According to the gyroscopic effect, as the inner and outer gimbals rotate, the direction of rotor's angular momentum is changed to produce the gyroscopic moment. Thus, the angular velocity accuracy of the gimbal systems determines the accuracy of the output torque of DGMSCMG [5]. Therefore, it is of great significance to improve the angular velocity accuracy of the gimbal servo control system.

The associate editor coordinating the review of this manuscript and approving it for publication was Kan Liu.

There are two main exogenous disturbances in the gimbal systems of DGCMG. Due to the strong gyroscopic effect, a significant nonlinear coupling torque is generated between the inner and outer gimbals [6]. Friction torque is another major factor affecting gimbal servo performance [7]. The gimbal servo systems always work at very low velocity, and the friction torque is non-linear, and it is very difficult to construct an accurate system model [8]. In addition, the endogenous disturbances caused by the unmodeled dynamics deteriorate the angular velocity servo performance.

In recent years, some literatures proposed some methods handling the exogenous problems in the gimbal system of CMG. A composite control compensation method based on simplified model is proposed in [9]. The effect of coupling torque is attenuated to some degree, but the complete elimination of coupling torque can not be realized. A simplified feedback linearization control method based on a modal separation approach [10], [11] and a differential geometry decoupling method [12] are proposed to decouple the DGCMG system. However, the control effect of these methods always suffer from the problem arising from the uncertainties on both the dynamic model and its parameters. In [8], a method that combines time delay control with internal model control

was proposed to compensate the nonlinear friction torque of gimbal system.

To estimate the exogenous and endogenous disturbances and compensate in an appropriate way is an effective method to suppress the influence of disturbances, and the disturbance observer is one of the key technical problems. In the last decades, as a tool for effectively estimating disturbance torque, extended state observer (ESO) which was originally proposed by professor Han, has been substantially developed [13]. Recently, the ESO-based control method was successfully employed in some applications such as motor control [14], [15], power converter [16], MEMS systems [17], robotic systems [18], [19], missile guidance [20] and other engineering practice [21], [22]. The parameter uncertainties, unmodeled dynamics and exogenous disturbances, which is regarded as the total disturbance, is extended as a new state of the system [23]. For a m-order system, the m+1 order ESO needs to be established and m+1 parameters are configured by bandwidth, which is an effective tuning method [24], [25].

One factor which severely limits the application of ESO is that if the order of system state equation is greater than 2, it is difficult to configure the parameters of the ESO that meets the system accuracy requirements in practical applications [26]. And corresponding parameters configuration approaches of ESO for a high-order system are still remained in discussions. In contrast, the theory and parameter configuration method of second-order ESO are relatively mature, and has been successfully applied in many industrial processes [27], [28]. To overcome this problem, a cascaded ESO (CESO) where the m+1 order ESO is replaced by m similar cascaded second-order ESOs with the same parameters was used to improve the accuracy of gimbal angular velocity [29]. However, the parameter configuration method for CESO is not analyzed.

In this paper, a reduced order CESO (RCESO) which is cascaded by two similar second-order ESOs is designed to estimate the unknown uncertainties and exogenous disturbances, and the parameter configuration method are given through frequency domain analysis. Sliding mode control (SMC) has been proven its robustness in practical control problems against a large class of perturbations and parameter uncertainties [30]–[32], and previous studies indicated that the SMC controller had better performance than feed back controller [33]. Considering the disturbance estimation errors of the total disturbance and with the aim of achieving total robustness and high precision angular velocity, this paper proposed a compound controller by putting together the design of using sliding surface and RCESO. Moreover, to eliminate steady-state error in the velocity tracking, integral action is augmented into the sliding-mode control law.

The proposed methodology has been tested by means of numerical simulations and experimental tests. This article is organized as follows: In section II, the model of DGMSCMG servo system is established and system disturbances are analyzed. Section III presents the design of RCESO, system stability analysis and parameter configuration method.

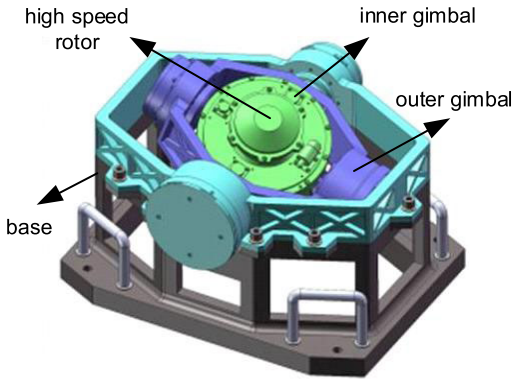

FIGURE 1. System structure of DGMSCMG.

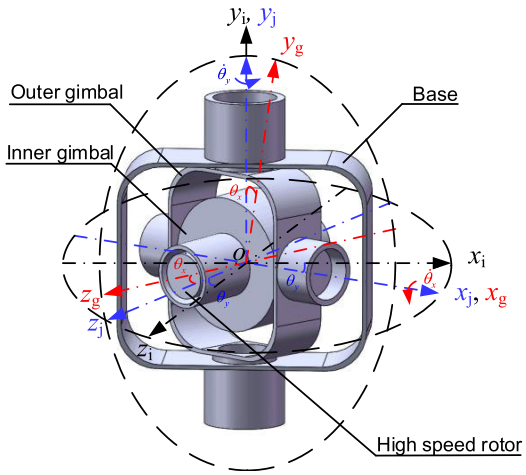

FIGURE 2. Definition of coordinate system of DGMSCMG.

In Section IV, the validity of the proposed method is verified by simulation and experiment. Some important conclusions are summarized in Section V.

II. DYNAMIC MODELING OF THE GIMBAL SYSTEMS AND DISTURBANCES ANALYSIS

As can be seen from the system structure shown in Figure.1, the DGMSCMG consists of the inner and outer gimbal servo systems and the magnetically suspended high speed rotor system, and the stator part of outer gimbal is fixed on the base. In addition, two resolvers are used to measure the angular position of the inner and outer gimbals respectively, and the angular velocities are calculated by the angular position. Meanwhile, the currents of the gimbal motors are obtained by two Hall current sensors.

The coordinates of DGMSCMG are defined in Figure. 2, where o is the geometry center of the stator in the gyro room, $ox_iy_iz_i$, $ox_jy_jz_j$ and $ox_gy_gz_g$ are the coordinates of base, outer gimbal and inner gimbal respectively. $ox_jy_jz_j$ roate around axis oy_i relative to $ox_iy_iz_i$, and the spinning angular of outer gimbal is defined as θ_y, spinning angular velocity is defined as $\dot{\theta}_y$. $ox_gy_gz_g$ rotate around ox_i axis relative to $ox_iy_iz_i$, and the spinning angular of inner gimbal is defined as θ_x, and the spinning angular velocity is defined as $\dot{\theta}_x$.

The dynamic equation of the inner and outer gimbal systems can be written as [29]

$$\begin{cases} T_x = K_x I_x = J_x \ddot{\theta}_x - J_x d_1 \\ T_y = K_y I_y = J_y \ddot{\theta}_y - J_y d_2 \end{cases} \tag{1}$$

where T_x and T_y are the output torque of the gimbal motors respectively, K_x and K_y are the torque coefficients, I_x and I_y are the current of the torque motors, J_x and J_y are equivalent inertia moment of the inner and outer gimbals, θ_x and θ_y are the spinning angle of the inner and outer gimbals, d_1 and d_2 are the lumped disturbances exerting on the inner and outer gimbal systems, respectively, with the following form

$$\begin{cases} d_1 = -\dfrac{1}{J_x}(H_z \dot{\theta}_y \cos\theta_x + F_x + \xi_x) \\ d_2 = -\dfrac{1}{J_y}(-H_z \dot{\theta}_x \cos\theta_x + F_y + \xi_y) \end{cases} \tag{2}$$

where F_x and F_y are the unmodeled dynamic of the inner and outer gimbals, ξ_x and ξ_y are the nonlinear friction torque of the inner and outer gimbals, $H_z\dot{\theta}_y \cos\theta_x$ and $-H_z\dot{\theta}_x \cos\theta_x$ are the coupling torque acting on the inner and outer gimbal systems, H_z is angular momentum of the magnetically suspended high speed rotor. The model about the motor of the inner and outer gimbal systems can be written as

$$\begin{cases} u_x = R_x I_x + L_x \dfrac{dI_x}{dt} + C_{ex}\dot{\theta}_x \\ u_y = R_y I_y + L_y \dfrac{dI_y}{dt} + C_{ey}\dot{\theta}_y \end{cases} \tag{3}$$

where u_x and u_y are the control voltage of the gimbal motors, R_x and R_y are the stator resistance of the torque motors, L_x and L_y are the inductance, C_{ex} and C_{ey} are the coefficients of back EMF. Define state variable as $\boldsymbol{x} = [x_{11}, x_{12}, x_{13}, x_{21}, x_{22}, x_{23}]^{\mathrm{T}} = [\theta_x, \dot{\theta}_x, I_x, \theta_y, \dot{\theta}_y, I_y]^{\mathrm{T}}$, and define control inputs of the inner and outer gimbal as u_x and u_y. The state space equation of the inner and outer gimbal systems is expressed as

$$\begin{cases} \dot{x}_{11} = x_{12} \\ \dot{x}_{12} = \dfrac{K_x}{J_x}x_{13} + d_1 \\ \dot{x}_{13} = -\dfrac{C_{ex}}{L_x}x_{12} - \dfrac{R_x}{L_x}x_{13} + \dfrac{1}{L_x}u_x \\ \dot{x}_{21} = x_{22} \\ \dot{x}_{22} = \dfrac{K_y}{J_y}x_{23} + d_2 \\ \dot{x}_{23} = -\dfrac{C_{ey}}{L_y}x_{22} - \dfrac{R_y}{L_y}x_{23} + \dfrac{1}{L_y}u_y \\ y_1 = x_{12} \\ y_2 = x_{22} \end{cases} \tag{4}$$

As can be seen from (4), control input u and disturbances d are not in the same channel, causing the mismatched problem. By introducing CESO to estimate the total disturbance and compensate the influence of it in the controller, the mismatched problem can be solved. However, (4) does not satisfy the traditional integral-chain form of CESO. Thus a coordinate transformation is introduced. The new coordinates are defined as

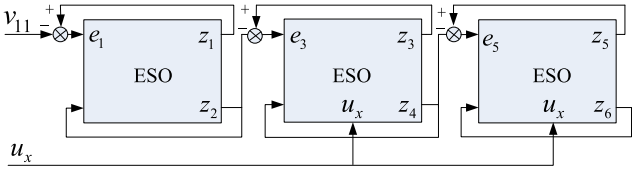

FIGURE 3. The structure of CESO.

$$\boldsymbol{v} = \begin{bmatrix} v_{11} \\ v_{12} \\ v_{13} \\ v_{21} \\ v_{22} \\ v_{23} \end{bmatrix} = \begin{bmatrix} x_{11} \\ x_{12} \\ \dfrac{K_x}{J_x}x_{13} + d_1 \\ x_{21} \\ x_{22} \\ \dfrac{K_y}{J_y}x_{23} + d_2 \end{bmatrix} \tag{5}$$

The state space equation of the gimbal system is rewritten as

$$\begin{cases} \begin{bmatrix} \dot{v}_{11} \\ \dot{v}_{12} \\ \dot{v}_{13} \end{bmatrix} = \begin{bmatrix} 0 & 1 & 0 \\ 0 & 0 & 1 \\ 0 & 0 & 0 \end{bmatrix} \begin{bmatrix} v_{11} \\ v_{12} \\ v_{13} \end{bmatrix} + \begin{bmatrix} 0 \\ 0 \\ b_x \end{bmatrix} u_x + \begin{bmatrix} 0 \\ 0 \\ f_x \end{bmatrix} \\ y_1 = v_{12} \\ \begin{bmatrix} \dot{v}_{21} \\ \dot{v}_{22} \\ \dot{v}_{23} \end{bmatrix} = \begin{bmatrix} 0 & 1 & 0 \\ 0 & 0 & 1 \\ 0 & 0 & 0 \end{bmatrix} \begin{bmatrix} v_{21} \\ v_{22} \\ v_{23} \end{bmatrix} + \begin{bmatrix} 0 \\ 0 \\ b_y \end{bmatrix} u_y + \begin{bmatrix} 0 \\ 0 \\ f_y \end{bmatrix} \\ y_2 = v_{22} \end{cases} \tag{6}$$

where v_{1j} and $v_{2j} (j = 1, 2, 3)$ are inner and outer gimbal system states respectively, y_1 and y_2 are the output of inner and outer gimbal system, $b_x = \frac{K_x}{J_x L_x}$, $b_y = \frac{K_y}{J_y L_y}$. and f_x, f_y are the total disturbance of inner and outer gimbal systems, respectively, which can be expressed as

$$\begin{cases} f_x = -\dfrac{K_x C_{ex}}{J_x L_x}v_{12} - \dfrac{R_x}{L_x}v_{13} + \frac{R_x}{L_x}d_1 + \dot{d}_1 \\ f_y = -\dfrac{K_y C_{ey}}{J_y L_y}v_{22} - \dfrac{R_y}{L_y}v_{23} + \frac{R_y}{L_y}d_2 + \dot{d}_2 \end{cases} \tag{7}$$

From (6), we can see that the inner and outer gimbal has a similar structure. Thus, we take the inner gimbal as an example to design the observer and corresponding control law in the following content.

III. COMPOSITE CONTROLLER DESIGN

A. DESIGN OF RCESO

According to [29], for a three-orders system, if we take the angular position v_{11} as the referenced input of CESO, then the linear CESO is cascaded by three similar second-order ESOs with the same parameters. The structure of CESO is shown as Figure. 3.

Since the control goal of the gimbal system is to achieve accurate angular velocity tracking control, we can use the v_{12}

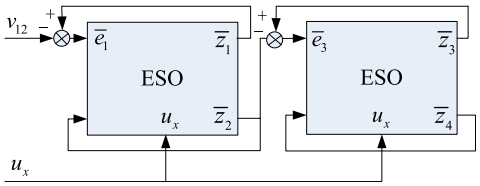

FIGURE 4. The structure of RCESO.

as the referenced input in the design of CESO. That means we can construct a reduced-ordered CESO, where we only need to estimate v_{12}, v_{13} and f_x. Thus, the traditional CESO can be transformed into a RCESO cascaded by two similar second-order ESOs, which simplifies the model of traditional CESO. The structure of RCESO is shown as Figure. 4.

We define the state variables of RCESO as $\bar{z} = [\bar{z}_1, \bar{z}_2, \bar{z}_3, \bar{z}_4]^{\mathrm{T}}$, where $\bar{z}_1$ is used to estimate v_{12}, $\bar{z}_2$ is used to estimate v_{13}, $\bar{z}_4$ is used to estimate f_x, and $\bar{z}_3$ is the intermediate variable. Estimation errors are defined as $\bar{e}_1 = \bar{z}_1 - v_{12}$, $\bar{e}_2 = \bar{z}_2 - v_{13}$, $\bar{e}_3 = \bar{z}_3 - \bar{z}_2$, $\bar{e}_4 = \bar{z}_4 - f_x$. The state equation of RCESO is described as follows

$$\begin{cases} \dot{\bar{z}}_1 = \bar{z}_2 - \bar{\beta}_1 \bar{e}_1 \\ \dot{\bar{z}}_2 = -\bar{\beta}_2 \bar{e}_1 + b_x u_x \\ \dot{\bar{z}}_3 = \bar{z}_4 - \bar{\beta}_1 \bar{e}_3 + b_x u_x \\ \dot{\bar{z}}_4 = -\bar{\beta}_2 \bar{e}_3 \end{cases} \tag{8}$$

where $\bar{\beta}_1$ and $\bar{\beta}_2$ are the parameters of RCESO. Subtracting (6) from (8), the error equation of RCESO is obtained as follows

$$\begin{cases} \dot{\bar{e}}_1 = \bar{e}_2 - \bar{\beta}_1 \bar{e}_1 \\ \dot{\bar{e}}_2 = -\bar{\beta}_2 \bar{e}_1 - f_x \\ \dot{\bar{e}}_3 = \bar{e}_4 - \bar{\beta}_1 \bar{e}_3 \\ \dot{\bar{e}}_4 = -\bar{\beta}_2 \bar{e}_3 - \dot{f}_x \end{cases} \tag{9}$$

Steady-state error of RCESO is

$$\bar{e}_1 = -\frac{f_x}{\bar{\beta}_2}, \quad \bar{e}_2 = -\frac{f_x \bar{\beta}_1}{\bar{\beta}_2}, \ \bar{e}_4 = -\frac{\dot{f}_x \bar{\beta}_1}{\bar{\beta}_2} \tag{10}$$

In the real DGCMG system, disturbances f_x is bounded, and its derivative $\dot{f}_x$ is also bounded. Thus, the steady-state error of CESO can be limited to a very small value by adjusting $\bar{\beta}_1$ and $\bar{\beta}_2$, and let $\bar{e}_4^* = \sup_{t>0} |\bar{e}_4|$.

However, whether the system stability and estimation performance of RCESO can be guaranteed after reducing the order of CESO needs to be further investigated in the following sections.

B. COMPOSITE CONTROLLER DESIGN AND SYSTEM STABILITY ANALYSIS

Through the previous analysis, it is known that the gimbal system can be decoupled into two independent subsystems by introducing a nonlinear disturbance observer. Taking the inner gimbal subsystem as an example, we design the controller of the system based on integral sliding mode approach.

Since the gimbal system is an angular velocity servo system, and the control target is to make the output angular velocity $\dot{\theta}$ tracking the command ω_{ref}, the sliding surface is given below.

$$s = \dot{v}_{12} - \dot{\omega}_{ref} + c_{1x}(v_{12} - \omega_{ref}) + c_{2x} \int_0^t (v_{12} - \omega_{ref}) dt \tag{11}$$

where c_{1x} and c_{2x} are positive constants to be designed. Invoking (6) with (11) yields

$$s = v_{13} - \dot{\omega}_{ref} + c_{1x}(v_{12} - \omega_{ref}) + c_{2x} \int_0^t (v_{12} - \omega_{ref}) dt \tag{12}$$

The proposed integral sliding mode control law is designed as

$$\begin{aligned} u_x = -{b_x}^{-1}(k_x \cdot sgn(s) &+ c_{1x}(v_{13} - \dot{\omega}_{ref}) \\ &+ c_{2x}(v_{12} - \omega_{ref}) - \ddot{\omega}_{ref} + \bar{z}_4) \end{aligned} \tag{13}$$

where k_x is the switching gain to be designed.

The stability of the closed-loop system is analyzed in the next based on the Lyapunov stability method. Taking the derivative of the sliding surface s described in (12), yields

$$\begin{aligned} \dot{s} &= \dot{v}_{13} - \ddot{\omega}_{ref} + c_{1x}(\dot{v}_{12} - \dot{\omega}_{ref}) + c_{2x}(v_{12} - \omega_{ref}) \\ &= -k_x \cdot sgn(s) - \bar{z}_4 + f_x \end{aligned} \tag{14}$$

Rewrite (9) to be

$$\dot{\bar{e}} = A_e \bar{e} + B_1 f_x + B_2 \dot{f}_x \tag{15}$$

where

$$A_e = \begin{bmatrix} -\beta_1 & 1 & 0 & 0 \\ -\beta_2 & 0 & 0 & 0 \\ 0 & 0 & -\beta_1 & 1 \\ 0 & 0 & -\beta_2 & 0 \end{bmatrix},$$

$$B_1 = \begin{bmatrix} 0 \\ -1 \\ 0 \\ 0 \end{bmatrix}, \quad and \quad B_2 = \begin{bmatrix} 0 \\ 0 \\ 0 \\ -1 \end{bmatrix}.$$

As we mentioned before, disturbances f_x and its derivation $\dot{f}_x$ are bounded in the real DGCMG system. Assuming that there exist bounded positive number ζ_1 and ζ_2 that make the inequality $f_x \le \zeta_1 \|\bar{e}_4\|$ and $\dot{f}_x \le \zeta_2 \|\bar{e}_4\|$ true.

Consider a candidate Lyapunov function as

$$V = \frac{1}{2} s^2 + \bar{e}^T P \bar{e} \tag{16}$$

where P is a unique symmetric positive definite matrix and satisfies

$${A_e}^T P + P A_e = -I \tag{17}$$

where A_e is Hurwitz and I is unit matrix.

Let $B_f = B_1 f_x + B_2 \dot{f}_x$, and we can get

$$\begin{aligned} \|B_f\| &= \|B_1 f_x + B_2 \dot{f}_x\| \\ &\le \|f_x\| + \|\dot{f}_x\| \\ &= \zeta_1 \|\bar{e}_4\| + \zeta_2 \|\bar{e}_4\| \\ &\le (\zeta_1 + \zeta_2) \|\bar{e}\| \end{aligned} \tag{18}$$

Combining (14), (15) and (18), the derivation of V can be achieved as

$$\begin{aligned}\dot{V} &= s\dot{s} + \dot{\bar{e}}^T P\bar{e} + \bar{e}^T P\dot{\bar{e}} \\ &= -k_x \|s\| + s\bar{e}_4 - \|\bar{e}\|^2 + 2\bar{e}^T P\left(B_1 f_x + B_2 \dot{f}_x\right) \\ &\le -k_x \|s\| + \|s\| \|\bar{e}_4\| - \|\bar{e}\|^2 + 2\bar{e}^T PB_f \\ &\le -(k_x - \|\bar{e}_4\|)\|s\| - (1 - 2\|P\|(\zeta_1 + \zeta_2))\|\bar{e}\|^2 \end{aligned} \quad (19)$$

Solve (17), we can obtain

$$P = \begin{bmatrix} \frac{\beta_2+1}{2\beta_1} & \frac{1}{2} & 0 & 0 \\ \frac{1}{2} & \frac{\beta_1{}^2+\beta_2+1}{2\beta_1\beta_2} & 0 & 0 \\ 0 & 0 & \frac{\beta_2+1}{2\beta_1} & \frac{1}{2} \\ 0 & 0 & \frac{1}{2} & \frac{\beta_1{}^2+\beta_2+1}{2\beta_1\beta_2} \end{bmatrix} \quad (20)$$

and $\|P\| = g(\beta_1, \beta_2) = \sqrt{\frac{(\beta_2+1)^2}{2\beta_1{}^2} + \frac{(\beta_1{}^2+\beta_2+1)^2}{2\beta_1{}^2\beta_2{}^2} + 1}$, which means that $\|P\|$ is the function of β_1 and β_2.

Therefore, we can chose parameters k_x, β_1 and β_2 that make equations $k_x > \bar{e}_4^*$ and $1 - 2\|P\|(\zeta_1 + \zeta_2) > 0$ true. Then, $\dot{V} < 0$ is guaranteed. Thus, the RCESO and the sliding surface is ensured to be convergent.

Let $\varepsilon = v_{12} - \omega_{ref}$, and then

$$s = \dot{\varepsilon}(t) + c_{1x}\varepsilon(t) + c_{2x}\int_0^t \varepsilon(\tau)d\tau = z(t) \quad (21)$$

Then, taking Laplace transform of (21), we have

$$\frac{\varepsilon(p)}{z(p)} = \frac{p}{p^2 + c_{1x}p + c_{2x}} \quad (22)$$

where p is the Laplace transform operator, $\varepsilon(p)$ and $z(p)$ are the Laplace transforms of $\varepsilon(t)$ and $z(t)$, respectively.

Then, according to the final value theorem, we can obtain

$$\varepsilon(\infty) = \lim_{p\to 0} \frac{p^2 z(p)}{p^2 + c_{1x}p + c_{2x}} \quad (23)$$

Because $\varepsilon(t)$ is bounded, we can know $z(t)$ is bounded from (21), which means $|z(t)| < z_{\max} < \infty$. Let $p = p_r + ip_i$, we have

$$\begin{aligned}|z(t)| &= \left|\int_0^\infty e^{-p\tau} z(\tau)d\tau\right| \le \int_0^\infty \left|e^{-p\tau} z(\tau)\right| d\tau \\ &\le z_{\max}\int_0^\infty \left|e^{-(p_r+ip_i)\tau}\right| d\tau \\ &\le z_{\max}\int_0^\infty \left|e^{-p_r\tau}\right| \left|e^{-ip_i\tau}\right| d\tau \\ &\le \frac{z_{\max}}{p_r} \end{aligned} \quad (24)$$

where e is the natural base.

$$\begin{aligned}\lim_{p\to 0}\left|p^2 z(p)\right| &\le \lim_{p_r\to 0, p_i\to 0}\left|(p_r + ip_i)^2 \frac{z_{\max}}{p_r}\right| \\ &\le \lim_{p_r\to 0}\left|p_r{}^2 \frac{z_{\max}}{p_r}\right| = 0 \end{aligned} \quad (25)$$

Combining (23), we can get $\lim_{t\to\infty} \varepsilon(t) = 0$, which means the whole closed-loop system is convergent and stable.

C. PARAMETER CONFIGURATION METHOD

1) ANALYSIS OF FREQUENCY PROPERTY

Combined the state equation of RCESO (8) with the state space equation of the gimbal system (6), the transfer function from f_x to $\bar{z}_4$ can be described as

$$G(s) = \frac{\bar{\beta}_2^2}{(s^2 + \bar{\beta}_1 s + \bar{\beta}_2)^2} \quad (26)$$

and its frequency property is

$$\phi(j\omega) = \frac{\bar{\beta}_2^2}{(\bar{\beta}_2 - \omega^2 + j\omega\beta_1)^2} \quad (27)$$

The amplitude-frequency and phase-frequency characteristics of which are

$$\begin{cases} A(\omega) = \dfrac{\bar{\beta}_2^2}{(\bar{\beta}_2 - \omega^2)^2 + \bar{\beta}_1^2\omega^2} \\ \psi(\omega) = -2arctg\dfrac{\bar{\beta}_1\omega}{\bar{\beta}_2 - \omega^2} \end{cases} \quad (28)$$

The following frequency property indexes are proposed to make the RCESO has good observational ability in a given frequency bandwidth $\omega \in [0, \omega_0]$.

$$\begin{cases} |A(\omega) - 1| \le A_0 \\ |\psi(\omega)| \le \psi_0 \end{cases} \quad (29)$$

where A_0 and ψ_0 are the maximum amplitude-frequency and phase-frequency error respectively allowed in $\omega \in [0, \omega_0]$.

From (29) and the stability condition of second order ESO $\bar{\beta}_1^2 > 4\bar{\beta}_2 > 4\omega_0$, we obtain $A(\omega)$ is monotonically decreased in $\omega \in [0, \omega_0]$. Besides, as can be seen from (29), the lagged phase angle increases with the increase of ω. Therefore, the amplitude-frequency error and the phase-frequency error simultaneously reach the maximum of the frequency property index (29) in $\omega = \omega_0$.

Thus, the following formulas (30) and (31) are established.

$$1 - A_0 \le \frac{\bar{\beta}_2^2}{(\bar{\beta}_2 - \omega_0^2)^2 + \bar{\beta}_1^2\omega_0^2} < 1 \quad (30)$$

$$2arctg\frac{\bar{\beta}_1\omega_0}{\bar{\beta}_2 - \omega_0^2} = \psi_0 \quad (31)$$

The final range of RCESO parameters $\bar{\beta}_1$, $\bar{\beta}_2$ which satisfy the frequency property index (30) can be obtained by taking the intersection of (30) and (31).

2) PARAMETER CONFIGURATION OF RCESO

In practical engineering, the phase angle error will not exceed 90°, which means the phase angle error is within the first quadrant. That can be expressed as

$$\bar{\beta}_2 - \omega_0^2 > 0 \quad (32)$$

As can be seen from (31), (32) and the stability conditions of RCESO, the result is shown as below.

(1) When $b_1 = \sqrt{(1-A_0)(1+tg^2\frac{\psi_0}{2})} > 1$, the result is expressed as

$$\begin{cases} \dfrac{a_2\omega_0^2}{a_2-1} < \bar{\beta}_2 \le \dfrac{b_1\omega_0^2}{b_1-1} \\ \bar{\beta}_1 = \dfrac{1}{\omega_0} a_1(\bar{\beta}_2 - \omega_0^2) \\ \bar{\beta}_1^2 > 4\bar{\beta}_2 > 4\omega_0 \end{cases} \tag{33}$$

where $a_1 = tg\frac{\psi_0}{2}$ and $a_2 = \sqrt{1+tg^2\frac{\psi_0}{2}}$.

(2) When $b_1 < 1$, the result is expressed as

$$\begin{cases} \bar{\beta}_2 > \dfrac{a_2\omega_0^2}{a_2-1} \\ \bar{\beta}_1 = \dfrac{1}{\omega_0} a_1(\bar{\beta}_2 - \omega_0^2) \\ \bar{\beta}_1^2 > 4\bar{\beta}_2 > 4\omega_0 \end{cases} \tag{34}$$

In (33) and (34), the stability conditions $\bar{\beta}_1^2 > 4\bar{\beta}_2 > 4\omega_0$ of RCESO can be described as $\bar{\beta}_2 > \frac{-b+\sqrt{b^2-4ac}}{2a}$, where $a = \frac{a_1^2}{4\omega_0^2}$, $b = -(2a\omega_0^2+1)$ and $c = a\omega_0^4$.

Therefore, for arbitrary ω_0, A_0 and ψ_0, where $\omega_0 > 0$, $0 < A_0 < 1$, $\psi_0 > 0$, if the parameters of RCESO satisfy any one of the conditions (33) and (34), the estimation of the total disturbance f_x in the RCESO system (8) satisfies the frequency property index (29).

3) ANALYSIS OF FREQUENCY RESPONSE

Figure. 5 shows the bode plots of disturbance estimation transfer function (26) under different frequency property index. As can be seen in Figure. 5, the bode plots of (26) satisfy the frequency property index well, where amplitude-frequency and phase-frequency error is within the given range. It is also obvious that the stricter the frequency property index is, the better performance the observer can achieve.

The plant structure can be described as Figure. 6(a) from the mathematical model of the plant, the transformed integral-chain form of which is shown as Figure. 6(b). Combined the plant structure with the control law of (13) and the model (8) of RCESO, the composite control system structure is obtained as Figure. 7, where the high frequency measured noise δ given by speed sensor to the observer is also included.

Figure. 7 can be converted to Figure. 8 where $G_r(s) = \frac{1}{s}\frac{(k_1+k_2s+k_3s^2)(s^2+\bar{\beta}_1s+\bar{\beta}_2)^2}{(s^2+\bar{\beta}_1s+\bar{\beta}_2)^2+k_3(s+\bar{\beta}_1)(s^2+\bar{\beta}_1s+\bar{\beta}_2)-\bar{\beta}_2^2}$, $G_p(s) = \frac{1}{s^2}$, $H_y(s) = \frac{(k_1+k_2s)(s^2+\bar{\beta}_1s+\bar{\beta}_2)^2+k_3\bar{\beta}_2s^2(s^2+\bar{\beta}_1s+\bar{\beta}_2)+\bar{\beta}_2^2s^3}{(s^2+\bar{\beta}_1s+\bar{\beta}_2)^2s+k_3(s+\bar{\beta}_1)(s^2+\bar{\beta}_1s+\bar{\beta}_2)-\bar{\beta}_2^2}$.

In order to evaluate the disturbance rejection action, the transfer function between the total disturbances $f_x(s)$ and the output angular speed $y_1(s)$ of the inner gimbal is described in (35).

$$\frac{y_1(s)}{f_x(s)} = \frac{G_p(s)}{1+H_y(s)G_p(s)} \tag{35}$$

Figure. 9 shows the bode plots of (35) under different parameter configurations. As we know, the smaller of the amplitude magnitude, the better disturbance rejection performance. Thus, from Figure. 9, we can see that with the better observer ability, the disturbance attenuation performance is better.

In terms of noise sensitivity, the transfer function from measured noise $\delta(s)$ to the output angular speed $y_1(s)$ of the

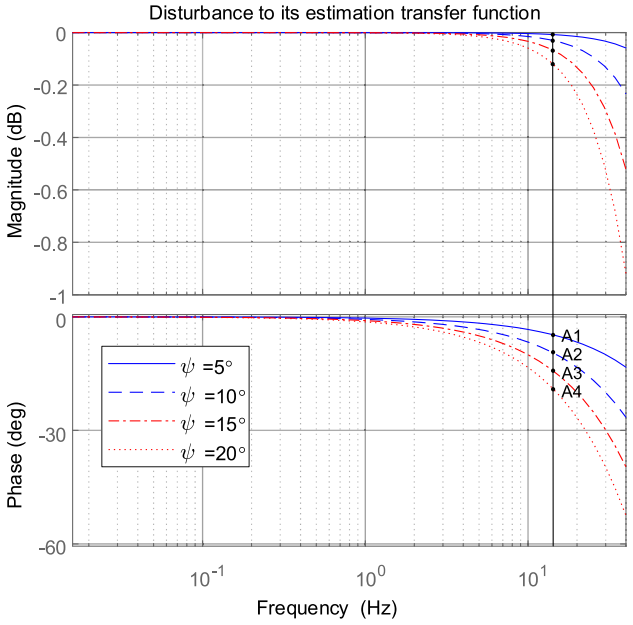

FIGURE 5. Comparison of disturbance estimation performance under different frequency property index.

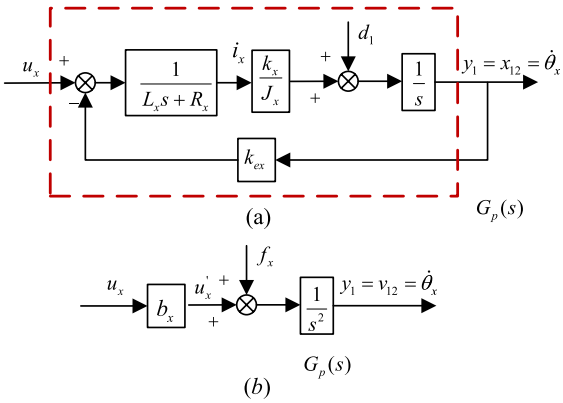

FIGURE 6. Structure of the plant.

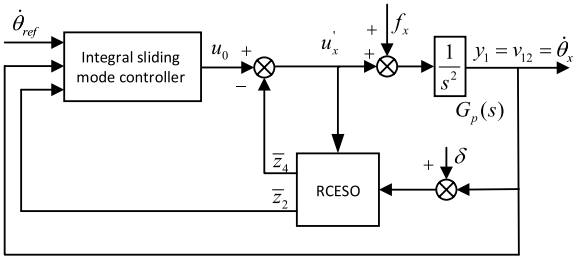

FIGURE 7. The structure of the whole control system with RCESO.

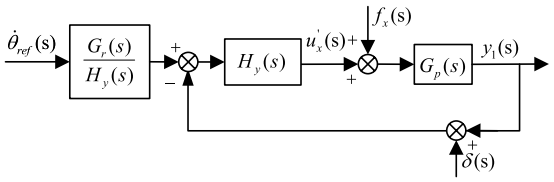

FIGURE 8. The block diagram of the whole control system with RCESO.

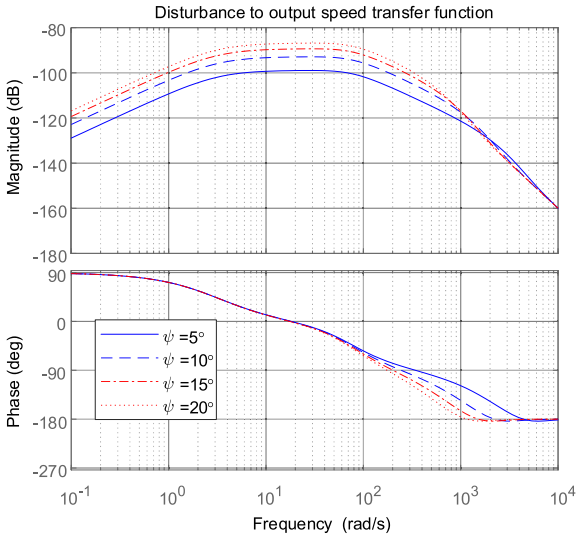

FIGURE 9. Comparison of disturbance attenuation between different parameters configuration.

inner gimbal is described as (36)

$$\frac{y_1(s)}{\delta(s)} = \frac{H_y(s)G_p(s)}{1 + H_y(s)G_p(s)} \tag{36}$$

The bode plots of (36) under different parameter configurations are shown in Figure. 10. It is shown that there is a trade off between the disturbance observer and the noise sensitivity.

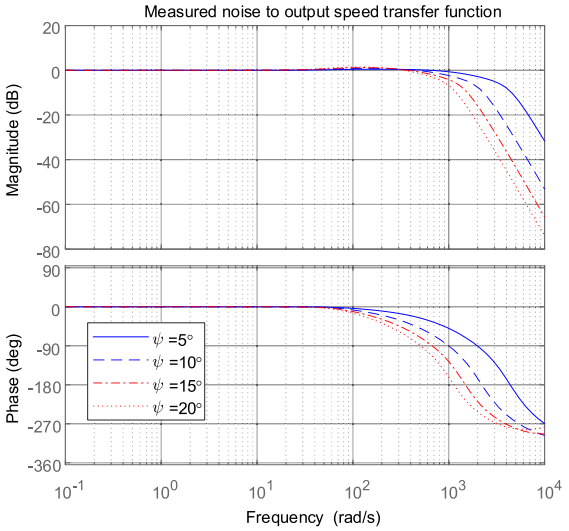

FIGURE 10. Comparison of noise sensitivity between different parameters configuration.

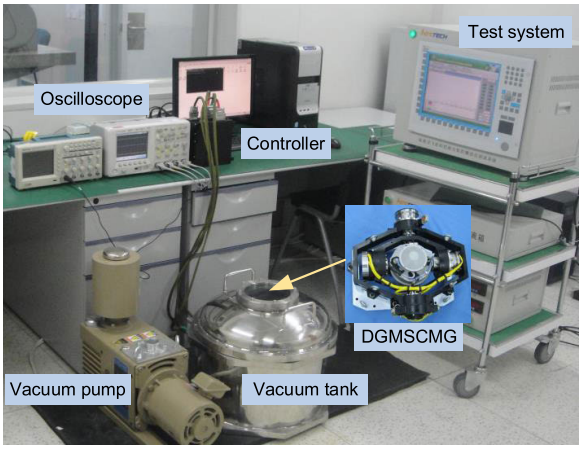

FIGURE 11. DGMSCMG prototype.

IV. SIMULATION AND EXPERIMENTAL RESULTS

A. SIMULATION AND EXPERIMENTAL SETUP

In order to verify the effectiveness and superiority of the parameter configuration method proposed in this paper in terms of disturbance estimation and rejection performance in DGCMG system, comparative simulations and experiments are carried out between the method used in [29] and the proposed method in this paper.

As can be seen from (8) and (13), there are 4 parameters to be designed in the system, which are $\bar{\beta}_1$, $\bar{\beta}_2$ of RCESO, and c_{1x}, c_{2x} of the controller. The controller parameters are related to the controller bandwidth ω_c, and configured as pole assignment method. And the controller bandwidth ω_c is related to the bandwidth requirment of gimbal angular speed. The frequency property indexes of the gimbal systems are selected as $A_0 = 0.1$, $\psi_0 = 10°$, then according to the parameter configuration method in this paper, (29) is a sufficient condition satisfying the frequency property index. From the above analysis, simulation parameters the same in the inner and outer gimbal system are configured as $c_{1x} = 3980$, $c_{2x} = 380$, $\bar{\beta}_1 = 4.3 \times 10^3$, $\bar{\beta}_2 = 4.7 \times 10^6$.

The inner and outer gimbal are set to be initially static and orthogonal in simulation and experiment since the coupling torque reaches the maximum in this condition. Furthermore, the Stribeck friction model, which is one of the most commonly used friction models in engineering, is introduced to the simulation to simulate the influence of nonlinear friction ξ_x and ξ_y in the gimbal system. The unmodeled dynamic F_x and F_y are set to be $0.01sin(188t)$ according to engineering debugging experience to the gimbal system of DGCMG. As the model of high frequency measured noise δ caused by position sensor, gaussian white noise is added to the simulation.

Experiments are conducted on the DGCMG prototype shown in Figure. 11, the parameters of which are given in TABLE 1. The controller of the gimbal servo system in Figure. 11 mainly includes DSP (TMS320F28335) and FPGA (A3P250) where the control algorithms are carried out.

TABLE 1. Main parameters of the system.

Parameter	value	Parameter	value
$J_x(kg.m^2)$	0.038	$R_x(\Omega)$	10
$J_y(kg.m^2)$	0.041	$R_y(\Omega)$	12
$K_x(N \cdot m/A)$	0.48	$L_x(mh)$	1.2
$K_y(N \cdot m/A)$	0.58	$L_y(mh)$	1.44
$C_{ex}(V/(rad/s)$	0.33	$H_z(N \cdot m \cdot s)$	20
$C_{ey}(V/(rad/s))$	0.38		

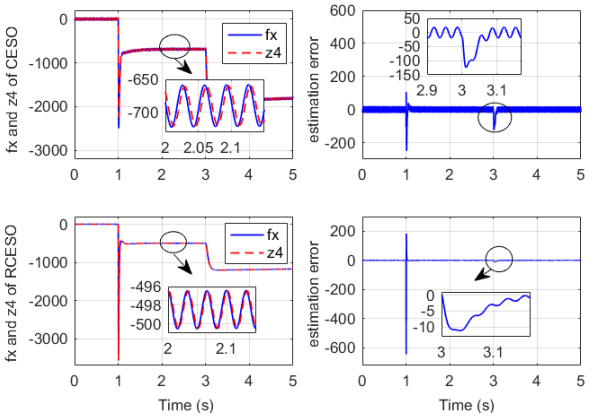

FIGURE 12. Comparative simulations of disturbance f_x and its estimation and estimation error of the inner gimbal under (a) CESO (b) RCESO without measured noise.

Both the sampling period of the angular and the servo periods are set to $1ms$.

B. SIMULATIONS OF DISTURBANCE ESTIMATION AND SUPPRESSION PERFORMANCE

In the following simulation and experimental results from Figure. 12 to Figure. 18, for the sake of clarity, let CESO denotes the parameter configuration method used in [29], RCESO denotes the parameter configuration method proposed in this paper, z_4 denotes the estimation value $\bar{z}_4$ of the total disturbance.

The inner and outer gimbal are given a step referenced angular speed signal of $5°/s$ when $t = 1s$ and $t = 3s$ respectively. Comparative simulations of disturbance f_x, its estimation $\bar{z}_4$ and estimation error of the inner gimbal under (a) CESO (b) RCESO are shown in Figure. 12 and Figure. 13.

Figure. 12 shows that $\bar{z}_4$ can perfectly estimate the 'total disturbance' f_x in (a) and (b), whereas estimation accuracy is significantly improved under the proposed configuration method. Furthermore, we see the steady-state observed error of RCESO is limited to a quite small value, which has been explained in formula (10). However, as can be seen from Figure. 13, when the measured noise is considered, the disturbance estimation of 'CESO' method is serious influenced.

Comparative simulations of step angular speed response waves of the inner and outer gimbal are shown in Figure. 14. As can be seen in Figure. 14, the outer and inner gimbal are subjected to the influence of the coupling torque, friction torque and unmodeled dynamics at $t = 1s$ and $t = 3s$ respectively when the referenced signal is given.

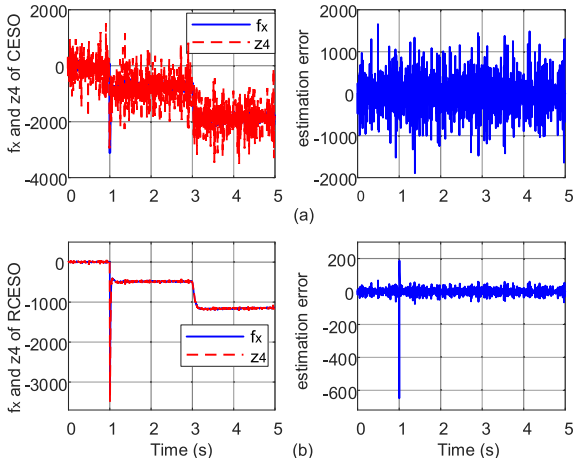

FIGURE 13. Comparative simulations of disturbance f_x and its estimation and estimation error of the inner gimbal under (a) CESO (b) RCESO with measured noise.

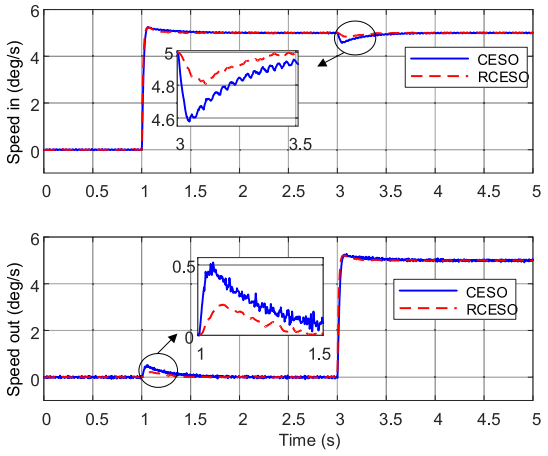

FIGURE 14. Comparative simulations of step angular speed response waves of the inner and outer gimbal.

Compared with the method of 'CESO', the angular speed fluctuation of outer gimbal using the parameters configuration method proposed in this paper is reduced from $0.51°/s$ to $0.22°/s$, and that of the inner gimbal is reduced from $0.41°/s$ to $0.20°/s$. Moreover, the overshoot of the step angular speed response waves of the inner and outer gimbal is smaller and the adjusting time is also shortened. Less angular speed fluctuation of the inner and outer gimbal indicates the proposed method has better disturbance rejection ability, which is also a proof to the disturbance estimation performance of RCESO in Figure. 13 from the aspect of time-domain.

To further verify the effectiveness from the aspect of time-domain of the proposed configuration method of RCESO which is deduced in frequency property, a sinusoidal speed signal with the amplitude of $5°/s$ and the frequency of $3Hz$ is given to the inner gimbal when $t = 0s$, and the same referenced sinusoidal speed signal is given to the outer gimbal when $t = 1s$. The disturbance estimation waves of RCESO of the outer gimbal system under the proposed configuration method are shown in Figure. 15.

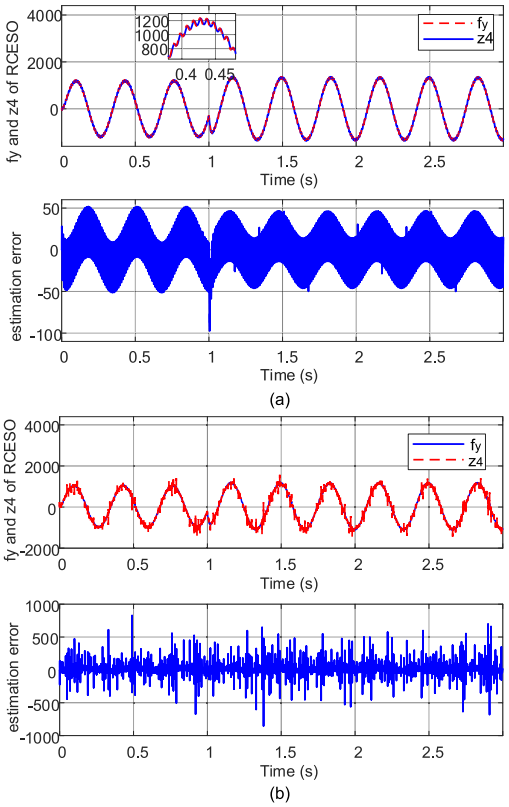

FIGURE 15. Simulation results of disturbance fy and its estimation and estimation error of RCESO of the outer gimbal under proposed configuration method (a) without measured noise (b) with measured noise.

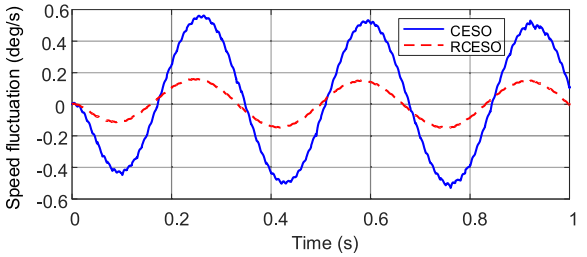

FIGURE 16. Comparative angular speed fluctuation of the outer gimbal.

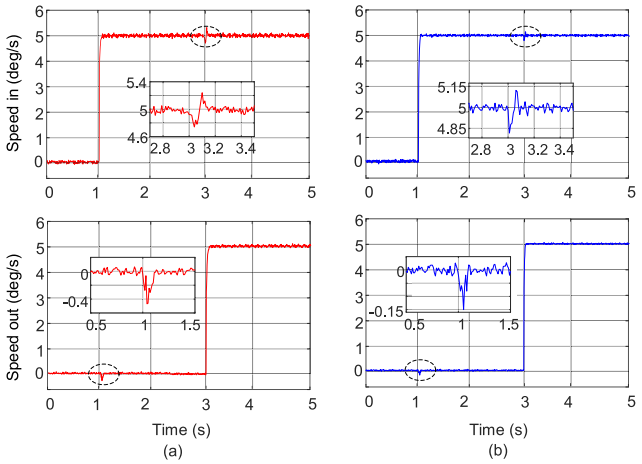

FIGURE 17. Experimental angular speed fluctuation of the outer and inner gimbal under (a) CESO (b) RCESO.

It can be observed from Figure. 15 that when the inner gimbal system is given a sinusoidal reference speed while the outer gimbal is locked between $0s$ and $1s$, the outer gimbal is subjected to the influence of sinusoidal periodic disturbances. In addition, when the outer gimbal starts at $t = 1s$, the disturbance acted on the outer gimbal increases. In spite of this, $\bar{z}_4$ can still perfectly estimate the 'total disturbance' f_y in the sinusoidal referenced signal, with the maximum amplitude error of 4% and the maximum phase delay of 3°, which can be calculated from the zoom-in boxes. The above analysis prove that the results satisfy the frequency property index (29).

In the design of the controller, the observed disturbance value is added to compensate for the influence of disturbance. To further explore the influence of residual disturbance on output angular speed of gimbal systems after disturbance compensation, we take the locked state (the reference angular speed is $0°/s$) within $1s$ of the outer gimbal under the sinusoidal periodic disturbances of Figure. 15 as an example to analyze the angular speed fluctuation. Comparative output angular speed fluctuations of the outer gimbal are shown in Figure. 16.

Combined Figure. 15 and Figure. 16, we can observe that, after compensating the influence of disturbance in the controller, the residual disturbance acted on the outer gimbal output is rather small, speed fluctuation of which is reduced to less than $0.18°/s$ with proposed method. Compared with the speed fluctuation of $0.56°/s$ with the method of 'CESO', the influence of disturbance on gimbal system output is significantly restrained. The above analysis verified the disturbance observation and disturbance rejection performance of the gimbal systems.

C. EXPERIMENTS OF DISTURBANCE REJECTION PERFORMANCE

In the above simulations, disturbance estimation and rejection performance are analyzed. In this section, to validate the effectiveness of the proposed parameters configuration method in terms of disturbance rejection performance in practical engineering, comparative experiments are conducted. Parameters configuration and referenced signals are totally the same as that in the simulations.

The angular speed fluctuation subjected to the influence of the other gimbal starts under step reference signal of the inner and outer gimbal are shown in Figure. 17.

As revealed by Figure. 17, $0.45°/s$ and $0.3°/s$ angular speed fluctuation occur in the outer and inner gimbals at $t = 1s$ and $t = 3s$ respectively with the 'CESO' method. Whereas the speed variation with the proposed method are reduced to $0.2°/s$ and $0.13°/s$ in outer and inner gimbal respectively. Besides, the steady accuracy is also improved. The experimental results demonstrate that the proposed method has better disturbance rejection performance.

The angular speed fluctuation of the outer gimbal is shown in Figure. 18. As shown in Figure. 18, the angular speed

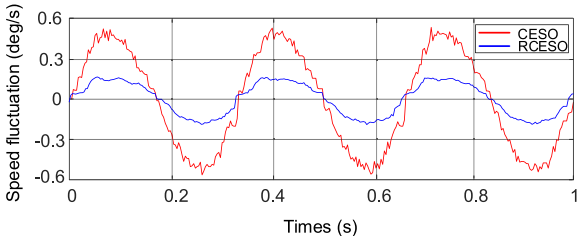

FIGURE 18. Experimental angular speed fluctuation of the outer gimbal.

fluctuation of the outer gimbal with the proposed method is decreased from $0.52°/s$ to $0.18°/s$, which demonstrate the rejection performance against mismatched disturbance.

The above experimental results comply well with the simulation results in Figure. 14 and Figure. 16. However, there is still some difference existing in gimbal output angular speed when compared with the simulation results. It is likely because that in simulation we only consider coupling torque, friction disturbance and unmodeled dynamics with certain frequency, whereas disturbances are more complicated in real system. Both the simulation and experimental results validate the disturbance rejection performance of the proposed method.

V. CONCLUSION

In this paper, a reduced-order cascade ESO-based sliding mode control scheme was proposed for disturbance rejection control of the gimbal system of DGCMG. By using angular speed as the referenced input of CESO, the traditional CESO cascaded by three similar second-order ESOs can be transformed into a RCESO cascaded by two similar second-order ESOs, which simplifies the model of traditional CESO. Furthermore, the transfer function from the total disturbance to its estimation in RCESO is obtained. And based on the above transfer function, the parameters of RCESO are configured to satisfy the frequency property index of RCESO. According to the non-null estimation error the total disturbance, a integral sliding mode controller is designed. Simulation and experimental results show this method perfectly meet the requirements of performance index, which demonstrate the estimation performance of RCESO from the aspect of time-domain. The proposed method can be applied to other practical engineering since multiple disturbances such as internal unmodeled dynamics, parameters change, external disturbances and other uncertain dynamics widely exist in engineer application. The proposed parameters configuration method is a way to configure the parameters of cascaded-formed ESOs, other configure methods can be explored in future studies.

REFERENCES

[1] V. Lappas, W. H. Steyn, and C. Underwood, "Design and testing of a control moment gyroscope cluster for small satellites," *J. Spacecraft Rockets*, vol. 42, no. 4, pp. 729–739, Jul. 2005.

[2] H. Li, S. Zheng, and H. Ren, "Self–correction of commutation point for high–speed sensorless BLDC motor with low inductance and nonideal back EMF," *IEEE Trans. Power Electron.*, vol. 32, no. 1, pp. 642–651, Jan. 2017.

[3] J. Ahmed and D. S. Bernstein, "Adaptive control of double–gimbal control–moment gyro with unbalanced rotor," *J. Guid., Control, Dyn.*, vol. 25, no. 1, pp. 105–115, Jan. 2002.

[4] S. Zheng, H. Li, B. Han, and J. Yang, "Power consumption reduction for magnetic bearing systems during torque output of control moment gyros," *IEEE Trans. Power Electron.*, vol. 32, no. 7, pp. 5752–5759, Jul. 2017.

[5] J. Fang, H. Li, and B. Han, "Torque ripple reduction in BLDC torque motor with nonideal back EMF," *IEEE Trans. Power Electron.*, vol. 27, no. 11, pp. 4630–4637, Nov. 2012.

[6] G. Wilson, "Double gimbal control moment gyroscope—gimbal control loop synthesis," in *Proc. Guid. Control Conf.*, vol. 1, Aug. 1975, p. 1108.

[7] M. Lu, S. Wang, W. Zheng, J. Liang, Y. Zhou, and N. Xia, "Ultra-low speed control strategy for SGCMG gimbal servo system," in *Proc. 26th Chin. Control Decision Conf. (CCDC)*, Changsha, China, May 2014. pp. 61–66.

[8] P. Cui, D. Zhang, S. Yang, and H. Li, "Friction compensation based on time–delay control and internal model control for a gimbal system in magnetically suspended CMG," *IEEE Trans. Ind. Electron.*, vol. 64, no. 5, pp. 3798–3807, May 2017.

[9] T. Wei, "Moving-gimbal effects compensation of double gimbal magnetically suspended control moment gyroscope based on compound control," *J. Mech. Eng.*, vol. 46, no. 2, p. 159, 2010.

[10] H. Li, S. Yang, and H. Ren, "Dynamic decoupling control of DGCMG gimbal system via state feedback linearization," *Mechatronics*, vol. 36, pp. 127–135, Jun. 2016.

[11] X. Chen and Y. Ren, "Modal decoupling control for a double gimbal magnetically gyroscope based on modal controller and feedback linearization method," *Int. J. Mech. Sci.*, vol. 228, no. 13, pp. 2303–2313, Sep. 2014.

[12] X. Chen and M. Chen, "Precise control of a magnetically suspended double-gimbal control moment gyroscope using differential geometry decoupling method," *Chin. J. Aeronaut.*, vol. 26, no. 4, pp. 1017–1028, Aug. 2013.

[13] J. Han, "From PID to active disturbance rejection control," *IEEE Trans. Ind. Electron.*, vol. 56, no. 3, pp. 900–906, Mar. 2009.

[14] L. Wang, M. Wang, B. Guo, Z. Wang, D. Wang, and Y. Li, "Analysis and design of a speed controller for electric load simulators," *IEEE Trans. Ind. Electron.*, vol. 63, no. 12, pp. 7413–7422, Dec. 2016.

[15] G. Li, W. Xu, J. Zhao, S. Wang, and B. Li, "Precise robust adaptive dynamic surface control of permanent magnet synchronous motor based on extended state observer," *IET Sci., Meas. Technol.*, vol. 11, no. 5, pp. 590–599, Aug. 2017.

[16] B. Sun and Z. Gao, "A DSP-based active disturbance rejection control design for a 1-kW H-bridge DC-DC power converter," *IEEE Trans. Ind. Electron.*, vol. 52, no. 5, pp. 1271–1277, Oct. 2005.

[17] Q. Zheng, L. Dong, D. Hui Lee, and Z. Gao, "Active disturbance rejection control for MEMS gyroscopes," *IEEE Trans. Control Syst. Technol.*, vol. 17, no. 6, pp. 1432–1438, Nov. 2009.

[18] J. Su, H. Ma, W. Qiu, and Y. Xi, "Task–independent robotic uncalibrated hand–eye coordination based on the extended state observer," *IEEE Trans. Syst. Man, Cybern. B, Cybern.*, vol. 34, no. 4, pp. 1917–1922, Aug. 2004.

[19] S. Talole, J. Kolhe, and S. Phadke, "Extended-state-observer-based control of flexible–joint system with experimental validation," *IEEE Trans. Ind. Electron.*, vol. 57, no. 4, pp. 1411–1419, Apr. 2010.

[20] Z. Zhu, D. Xu, J. Liu, and Y. Xia, "Missile guidance law based on extended state observer," *IEEE Trans. Ind. Electron.*, vol. 60, no. 12, pp. 5882–5891, Dec. 2013.

[21] X. Song, J. Fang, B. Han, and S. Zheng, "Adaptive compensation method for high–speed surface PMSM sensorless drives of EMF–based position estimation error," *IEEE Trans. Power Electron.*, vol. 31, no. 2, pp. 1438–1449, Feb. 2016.

[22] J. Han, "Auto-disturbance rejection control and its applications," *Control Decis.*, vol. 13, no. 1, pp. 23–33, Jan. 1998.

[23] W. Xue, W. Bai, S. Yang, K. Song, Y. Huang, and H. Xie, "ADRC with adaptive extended state observer and its application to Air-fuel ratio control in gasoline engines," *IEEE Trans. Ind. Electron.*, vol. 62, no. 9, pp. 5847–5857, Sep. 2015.

[24] Z. Gao, "Scaling and bandwidth-parameterization based controller tunning," in *Proc. Amer. Control Conf.*, 2003, pp. 4989–4996.

[25] Z. Gao, "Active disturbance rejection control: A paradigm shift in feedback control system design," in *Proc. Amer. Control Conf.*, , Jun. 2006, pp. 2399–2405.

[26] R. Zhang and J. Han, "Auto-disturbances rejection controller constructed by cascade extended state observer," *Control Decis.*, vol. 15, no. 1, pp. 122–124, Jan. 2000.

[27] X. Chen, D. Li, Z. Gao, and C. Wang, "Tuning method for second-order active disturbance rejection control," in *Proc. 30th Chin. Control Conf.*, Yantai, China, Jan. 2000, pp. 6322–6327.
[28] J. Han and R. Zhang, "Error analysis of the second order ESO," *J. Syst. Sci. Math. Scis.*, vol. 19, no. 4, pp. 465–471, 1999.
[29] H. Li, S. Zheng, and X. Ning, "Precise control for gimbal system of double gimbal control moment gyro based on cascade extended state observer," *IEEE Trans. Ind. Electron.*, vol. 64, no. 6, pp. 4653–4661, Jun. 2017.
[30] B. Jiang, H. R. Karimi, Y. Kao, and C. Gao, "A novel robust fuzzy integral sliding mode control for nonlinear Semi–Markovian Jump T-S fuzzy systems," *IEEE Trans. Fuzzy Syst.*, vol. 26, no. 6, pp. 3594–3604, Dec. 2018.
[31] M. A. M. Cheema, J. E. Fletcher, M. Farshadnia, and M. F. Rahman, "Sliding mode based combined speed and direct thrust force control of linear permanent magnet synchronous motors with first–order plus integral sliding condition," *IEEE Trans. Power Electron.*, vol. 34, no. 3, pp. 2526–2538, Mar. 2019.
[32] Z. Ma and P. Huang, "Discrete-time sliding mode control for deployment of tethered space robot with only length and angle measurement," *IEEE Trans. Aerosp. Electron. Syst.*, vol. 14, no. 8, pp. 1–11, May 2019.
[33] J.-H. Fang, F. Guo, Z. Chen, and J.-H. Wei, "Improved sliding-mode control for servo-solenoid valve with novel switching surface under acceleration and jerk constraints," *Mechatronics*, vol. 43, pp. 66–75, May 2017.
[34] S. Zhao and Z. Gao, "An active disturbance rejection based approach to vibration suppression in two–inertia systems," *Asian J. Control*, vol. 15, no. 2, pp. 350–362, Mar. 2013.
[35] S. Li, J. Yang, W.-H. Chen, and X. Chen, "Generalized extended state observer based control for systems with mismatched uncertainties," *IEEE Trans. Ind Electron.*, vol. 59, no. 12, pp. 4792–4802, Dec. 2010.
[36] A. Isidori, *Nonlinear Control System*, London, U.K.: Springer, 1999.
[37] H. K. Khalil, *Nonlinear Systems*. Upper Saddle River, NJ, USA: Prentice-Hall, 1995.

HAITAO LI received the B.S. degree in automation and the M.S. degree in mechatronics from Shandong University, Jinan, China, in 2002 and 2005, respectively, and the Ph.D. degree in precision instruments and machinery from Beihang University, Beijing, China, in 2009.

He is currently with the School of Instrumentation Science and Optoelectronics Engineering, Beihang University, and also with the Beijing Engineering Research Center of High-Speed Magnetically Suspended Motor Technology and Application, Beihang University. His main research interests include magnetically suspended control moment gyro and its nonlinear control.

JIANGKUN YU received the B.S. degree in automation from the China University of Petroleum, Qingdao, China. He is currently pursuing the master's degree in instrumental science and technology with the Beihang University, Beijing, China. His research interest includes motor servo control and speed precision control of gimbal system in magnetically suspended control moment gyro.